Available online at www.sciencedirect.com
ScienceDirect
Journal of Computational Physics 227 (2007) 1286–1305
JOURNAL OF COMPUTATIONAL PHYSICS
www.elsevier.com/locate/jcp

Statistical mechanics of Arakawa's discretizations ☆

Svetlana Dubinkina, Jason Frank *

CWI, P.O. Box 94079, 1090 GB Amsterdam, The Netherlands

Received 26 July 2007; received in revised form 30 August 2007; accepted 4 September 2007
Available online 14 September 2007

Abstract

The results of statistical analysis of simulation data obtained from long time integrations of geophysical fluid models greatly depend on the conservation properties of the numerical discretization used. This is illustrated for quasi-geostrophic flow with topographic forcing, for which a well established statistical mechanics exists. Statistical mechanical theories are constructed for the discrete dynamical systems arising from three discretizations due to Arakawa [Arakawa, Computational design for long-term numerical integration of the equations of fluid motion: two-dimensional incompressible flow. Part I. J. Comput. Phys. 1 (1966) 119–143] which conserve energy, enstrophy or both. Numerical experiments with conservative and projected time integrators show that the statistical theories accurately explain the differences observed in statistics derived from the discretizations.

PACS: 65M06; 65P10; 86A10; 82B99

Keywords: Conservative discretizations; Statistical mechanics; Geometric numerical integration; Quasi-geostrophic flow; Geophysical fluid dynamics

1. Introduction

In applications such as weather and climate predictions, long numerical simulations are run for dynamical systems that are known to be chaotic, and for which it is consequently impossible to simulate a particular solution with any accuracy in the usual sense of numerical analysis. Instead, the goal of such simulations is to obtain a data set suitable for computing statistical averages or otherwise to sample the probability distribution associated with the continuous problem.

Different numerical discretizations have very different discrete dynamics, however. Recent work on geometric integration [24,25,7,10] relies on backward error analysis, in which the numerical solution generated by a given method is viewed as the exact solution of a perturbed problem. The properties of different discrete

☆ The investigations were in part supported by the Research Council for Earth and Life Sciences (ALW) with financial aid from the Netherlands Organization for Scientific Research (NWO).
* Corresponding author.
E-mail addresses: dubinkin@cwi.nl (S. Dubinkina), jason@cwi.nl (J. Frank).

0021-9991/$ - see front matter
doi:10.1016/j.jcp.2007.09.002

dynamics become more pronounced when the numerical map is iterated over a very large number of time steps. Therefore, it is important to establish the influence that a particular choice of method has on the statistical results obtained from simulations. Ideally, one would like to determine criteria which a method should satisfy to yield meaningful statistics and to understand statistical accuracy in terms of discretization parameters.

To that end, in this paper we consider three related discretizations for an ideal fluid in vorticity-stream function form, originally proposed by Arakawa [2]. The three discretizations conserve discrete approximations of energy, enstrophy or both. We analyze the three methods through appropriate (trivial) modifications of the statistical mechanics theory of quasi-geostrophic flow over topography, based on the original work of Kraichnan [9], Salmon et al. [22] and Carnevale and Frederiksen [3], and recently expounded in Majda and Wang [12]. The resulting theories predict entirely different statistical behavior for the three methods. Numerical experiments with conservative and projected time integrators agree with the statistical predictions, confirming that the conservation properties of a discretization define the backdrop, or climatic mean, against which the dynamics takes place.

It should be mentioned at the outset that the energy–enstrophy statistical theory is a model and is known to be incomplete. In [1], Abramov and Majda show that nonzero values of the third moment of potential vorticity can cause significant deviation from the statistical predictions. In Section 6 we use the numerical setup of [1] to facilitate comparison with their results. We wish to stress, however, that the focus of this article is not the statistical mechanics of ideal fluids *per se*, but rather the application of statistical mechanics as a tool for the numerical analysis of discretizations.

In Section 2 we briefly recall the quasi-geostrophic potential vorticity equation and its conservation properties. Section 3 we review Arakawa's discretizations, their conservation properties, and prove that all of these define divergence-free vector fields. In Section 4, the equilibrium statistical mechanical theories are developed for the three discretizations. Most of this section is simply a summary of material in Chapters 7 and 8 of [12] for the energy–enstrophy theory. Once established, it is a simple matter to extend the results to the cases in which only one of these quantities is conserved, and we do this in Section 4.4. Time integration aspects are discussed in Section 5. The numerical experiments confirming the statistical predictions are presented in Section 6.

2. The quasi-geostrophic model

This paper addresses the statistical mechanics of conservative discretizations of the quasi-geostrophic potential vorticity model (QG) on a doubly periodic domain, $\Omega = \{\boldsymbol{x} = (x, y) | x, y \in [0, 2\pi)\}$. The QG equation [18,19] is

$$q_t = \mathcal{J}(q, \psi), \tag{1a}$$

$$\Delta\psi = q - h, \tag{1b}$$

where the potential vorticity (PV) $q(\boldsymbol{x}, t)$, the stream function $\psi(\boldsymbol{x}, t)$ and the orography $h(\boldsymbol{x})$ are scalar fields, periodic in x and y with period 2π. The Laplace operator is denoted by Δ, and the operator $\mathcal{J}$ is defined by

$$\mathcal{J}(q, \psi) = q_x\psi_y - q_y\psi_x. \tag{2}$$

The QG equation is a Hamiltonian PDE [15] having Poisson bracket

$$\{\mathcal{F}, \mathcal{G}\} = \int q\mathcal{J}\left(\frac{\delta\mathcal{F}}{\delta q}, \frac{\delta\mathcal{G}}{\delta q}\right)\mathrm{d}\boldsymbol{x} \tag{3}$$

and Hamiltonian functional

$$\mathcal{E}[q] = -\frac{1}{2}\int \psi \cdot (q - h)\mathrm{d}\boldsymbol{x}. \tag{4}$$

The Poisson bracket is degenerate with Casimir invariants the generalized enstrophies $\mathcal{Q}[q] = \int f(q)\mathrm{d}\boldsymbol{x}$ for arbitrary function f. The most important of these are the total circulation

$$\mathcal{C}[q] = \int q \mathrm{d}\boldsymbol{x} \tag{5}$$

and the second moment of vorticity, i.e. the enstrophy

$$\mathcal{Z}[q] = \frac{1}{2}\int q^2 \mathrm{d}\boldsymbol{x}. \tag{6}$$

3. Spatial semi-discretization

We first consider the discretization of (1) in space only. The resulting system of ordinary differential equations will be referred to as the semi-discretization, and we will primarily be concerned with its analysis and statistical mechanics.

When discretizing Hamiltonian PDEs, it is advisable to consider the discretizations of the Poisson bracket and the Hamiltonian separately. As noted in [13], if a discrete Poisson bracket can be constructed to maintain skew-symmetry and satisfy the Jacobi identity, then any quadrature for the Hamiltonian will yield a semi-discretization that constitutes a Hamiltonian ODE, and consequently will conserve energy and (possibly some subclass of) Casimirs. From the point of view of statistical mechanics, it is *also* natural to consider the discretizations of the bracket and the Hamiltonian separately. The bracket ensures the conservation of energy and enstrophy and preservation of volume, which are necessary ingredients for the *existence* of a statistical theory at all. But only the conserved quantities themselves enter into the probability distribution. Thus the *predictions* of the theory depend only on the discretization of these conserved quantities. The discretization of the Hamiltonian (4) amounts to a choice for the discrete Laplacian in (1b) and will be treated in Section 3.1. The bracket will be discretized with (generalized) Arakawa schemes in Section 3.2.

For Eulerian fluid models, the only known discretization with Poisson structure is the sine-bracket truncation of Zeitlin [26], which is limited to 2D, incompressible flows on periodic geometry. This truncation conserves M polynomial enstrophies on an $M \times M$ grid. Its statistics are investigated in [1]. For more general fluid problems, no Poisson discretizations are available. In lieu of a semi-discretization with Poisson structure, one may attempt to construct discretizations which conserve desired first integrals and are volume preserving. The flow of energy is important for statistics, and the spatial discretization determines the local flow. In numerical weather prediction, energy conserving discretizations were advocated by Lorenz in 1960 [11]. Motivated by Lorenz's work, Arakawa [2] constructed discretizations that conserved energy, enstrophy or both. As we will see, these discretizations are also all volume preserving.

We discretize (1) on a uniform $M \times M$ grid. Let $\Delta x = \Delta y = 2\pi/M$ and consider a grid function $\boldsymbol{q}(t) \in R^{M\times M}$, with components $q_{i,j}(t) \approx q(i\Delta x, j\Delta y, t)$, $i,j = 0,\ldots,M-1$, where periodicity is realized by identifying the indices M and 0. We think of $\boldsymbol{q}$ as a vector in an M^2-dimensional phase space; that is, we identify R^{M^2} and $R^{M\times M}$, and use vector notation, e.g. $\boldsymbol{\Psi}^{\mathrm{T}}\boldsymbol{q}$ for the vector inner product of two such vectors.

3.1. Spectral solution of the stream function

The linear elliptic PDE (1b) is solved using the Fourier spectral method. Let the Fourier transform of $\boldsymbol{q} \in R^{M\times M}$ be defined by

$$\hat{\boldsymbol{q}} = \mathcal{F}\boldsymbol{q} \Longleftrightarrow \hat{q}_{k,\ell} = \frac{1}{M}\sum_{i,j=0}^{M-1} q_{i,j} \mathrm{e}^{-\mathrm{i}(ik+j\ell)}, \quad k,\ell = -M/2+1,\ldots,M/2. \tag{7}$$

The inverse transform is $\mathcal{F}^{-1} = \mathcal{F}^*$, and Parseval's identity reads

$$\sum_{i,j} q_{i,j}^2 = \sum_{k,\ell} |\hat{q}_{k,\ell}|^2.$$

Eq. (1b) is solved exactly in Fourier-space. Denote the discrete Laplace operator by Δ_M:

$$\Delta_M \boldsymbol{\psi} = \boldsymbol{q} - \boldsymbol{h} \Longleftrightarrow -(k^2+\ell^2)\hat{\psi}_{k,\ell} = \hat{q}_{k,\ell} - \hat{h}_{k,\ell}, \quad k,\ell = -M/2+1,\ldots,M/2. \tag{8}$$

This relation is solved for stream function field $\boldsymbol{\psi}$ with mean zero. The inverse Laplacian restricted to the hyperplane $\hat{\psi}_{0,0} \equiv 0$ is denoted by Δ_M^{-1}, i.e.

$$\boldsymbol{\psi} = \Delta_M^{-1}(\boldsymbol{q} - \boldsymbol{h}) \Longleftrightarrow \hat{\psi}_{k,\ell} = \begin{cases} 0, & k = \ell = 0, \\ -(\hat{q}_{k,\ell} - \hat{h}_{k,\ell})/(k^2 + \ell^2), & \text{otherwise.} \end{cases}$$

3.2. Arakawa's discretizations

Arakawa [2] constructed finite difference discretizations of (2) that preserve discrete versions of energy (4), enstrophy (6) or both. We consider generalizations to Arakawa's discretizations with the Nambu bracket approach of [21].

Let D_x and D_y denote discretization matrices that (i) are skew symmetric: $D_x^{\mathrm{T}} = -D_x$, $D_y^{\mathrm{T}} = -D_y$ and (ii) approximate the first derivative in x and y, respectively:

$$(D_x\boldsymbol{q})_{i,j} \approx q_x(i\Delta x, j\Delta y), \quad (D_y\boldsymbol{q})_{i,j} \approx q_y(i\Delta x, j\Delta y).$$

Arakawa's classical discretizations [2] use the central differences

$$(D_x\boldsymbol{q})_{i,j} = \frac{q_{i+1,j} - q_{i-1,j}}{2\Delta x}, \quad (D_y\boldsymbol{q})_{i,j} = \frac{q_{i,j+1} - q_{i,j-1}}{2\Delta y}, \tag{9}$$

and these will also be used in our numerical experiments. However, the statistical predictions in Section 4 remain unchanged for a different choice of (skew-symmetric) D_x and D_y.

Denote the element-wise product of two vectors by $(\boldsymbol{u} * \boldsymbol{v})_{i,j} = u_{i,j}v_{i,j}$. The scalar product

$$\boldsymbol{u}^{\mathrm{T}}(\boldsymbol{v} * \boldsymbol{w}) = \sum_{i,j} u_{i,j}v_{i,j}w_{i,j} \tag{10}$$

is fully symmetric with respect to the vectors $\boldsymbol{u}$, $\boldsymbol{v}$ and $\boldsymbol{w}$.

Arakawa's discretizations can be viewed as discrete approximations to the equivalent formulations of (2)

$$\begin{aligned} \mathcal{J}(q,\psi) &= q_x\psi_y - q_y\psi_x, \\ \mathcal{J}(q,\psi) &= \partial_x(q\psi_y) - \partial_y(q\psi_x), \\ \mathcal{J}(q,\psi) &= \partial_y(q_x\psi) - \partial_x(q_y\psi) \end{aligned}$$

and are given by

$$J_0(\boldsymbol{q},\boldsymbol{\psi}) = (D_x\boldsymbol{q}) * (D_y\boldsymbol{\psi}) - (D_y\boldsymbol{q}) * (D_x\boldsymbol{\psi}), \tag{11}$$

$$J_E(\boldsymbol{q},\boldsymbol{\psi}) = D_x(\boldsymbol{q} * D_y\boldsymbol{\psi}) - D_y(\boldsymbol{q} * D_x\boldsymbol{\psi}), \tag{12}$$

$$J_Z(\boldsymbol{q},\boldsymbol{\psi}) = D_y(\boldsymbol{\psi} * D_x\boldsymbol{q}) - D_x(\boldsymbol{\psi} * D_y\boldsymbol{q}) \tag{13}$$

and the average of these

$$J_{EZ}(\boldsymbol{q},\boldsymbol{\psi}) = \frac{1}{3}[J_0(\boldsymbol{q},\boldsymbol{\psi}) + J_E(\boldsymbol{q},\boldsymbol{\psi}) + J_Z(\boldsymbol{q},\boldsymbol{\psi})]. \tag{14}$$

That is, the semi-discretizations are defined by (8) and

$$\frac{\mathrm{d}}{\mathrm{d}t}\boldsymbol{q} = J(\boldsymbol{q},\boldsymbol{\psi}) \tag{15}$$

for J taken to be one of (11)–(14).

The Arakawa schemes are interesting for us, because they are all based on the standard central difference operators applied in various 'conservation forms' and hence, for short simulations with smooth solutions, there is often little noticeable difference between different discretizations. They might be expected to yield similar statistics. On the contrary, the long-term statistics differ greatly.

The conservation properties of these three discretizations were established for the case of second order differences (9) in [2]. The case (14) has been generalized using the Nambu bracket formalism [16,17,21]. Define the associated brackets (the gradients are with respect to $\boldsymbol{q}$)

$$\{F,G,H\}_0 = -\nabla F^{\mathrm{T}} J_0(\nabla G, \nabla H), \tag{16}$$

$$\{F,G,H\}_E = -\nabla F^{\mathrm{T}} J_E(\nabla G, \nabla H), \tag{17}$$

$$\{F,G,H\}_Z = -\nabla F^{\mathrm{T}} J_Z(\nabla G, \nabla H), \tag{18}$$

$$\{F,G,H\}_{EZ} = \frac{1}{3}(\{F,G,H\}_0 + \{F,G,H\}_E + \{F,G,H\}_Z) \tag{19}$$

for arbitrary differentiable $F(\boldsymbol{q})$, $G(\boldsymbol{q})$, $H(\boldsymbol{q}) : R^{M^2} \to R$.

The derivative $\frac{\mathrm{d}F}{\mathrm{d}t}$ of any function $F(\boldsymbol{q})$ along a solution $\boldsymbol{q}(t)$ to the discrete equations (15) is given by the associated bracket of F with Z_M and E_M:

$$\frac{\mathrm{d}F}{\mathrm{d}t} = \{F, Z_M, E_M\}, \tag{20}$$

where E_M and Z_M are discrete approximations to the energy

$$E_M(\boldsymbol{q}) = -\frac{1}{2}\boldsymbol{\psi}^{\mathrm{T}}(\boldsymbol{q}-\boldsymbol{h})\Delta x\Delta y = \frac{1}{2}\sum_{k,\ell}(k^2+\ell^2)|\hat{\psi}_{k,\ell}|^2\Delta x\Delta y \tag{21}$$

and enstrophy

$$Z_M(\boldsymbol{q}) = \frac{1}{2}\boldsymbol{q}^{\mathrm{T}}\boldsymbol{q}\Delta x\Delta y = \frac{1}{2}\sum_{k,\ell}|\hat{q}_{k,\ell}|^2\Delta x\Delta y. \tag{22}$$

This fact can be used to prove the conservation properties of the various discretizations.

The proofs rely on the antisymmetry of (16) with respect to its last two arguments,

$$\{F,G,H\}_0 = -\{F,H,G\}_0,$$

as well as the identities

$$\{F,G,H\}_E = \{G,H,F\}_0, \quad \{F,G,H\}_Z = \{H,F,G\}_0,$$

all of which follow from the skew-symmetry of D_x and D_y and the symmetry of (10).

Taking $F \equiv E_M$ in (20), it follows that for J_E,

$$\frac{\mathrm{d}E_M}{\mathrm{d}t} = \{E_M, Z_M, E_M\}_E = \{Z_M, E_M, E_M\}_0 = 0.$$

Similarly, taking $F \equiv Z_M$ in (20), it follows that for J_Z,

$$\frac{\mathrm{d}Z_M}{\mathrm{d}t} = \{Z_M, Z_M, E_M\}_Z = \{E_M, Z_M, Z_M\}_0 = 0.$$

The bracket (19) is fully antisymmetric in all three arguments (hence it is a proper Nambu bracket), and therefore conserves both E_M and Z_M. Finally, taking $F = C_M = \sum_{i,j} q_{i,j}\Delta x\Delta y$, one can show that all of the discretizations (16)–(19) conserve total circulation.

In reference to their conservation properties, we will refer to the discretizations (11)–(14) as the 0, E, Z and EZ discretizations, respectively.

One can check that a solution of the form $\boldsymbol{q} = \mu\boldsymbol{\psi}$, μ a scalar, is an exact steady state for the 0 and EZ discretizations. Such a solution is not, in general, a steady state solution for the E and Z discretizations. However, the limit cases $\{\boldsymbol{\psi} \equiv 0, \boldsymbol{q} = \boldsymbol{h}\}$ and $\{\boldsymbol{q} \equiv 0, \boldsymbol{\psi} = -\Delta_M^{-1}\boldsymbol{h}\}$ obviously *are* steady states to those discretizations.

3.3. Volume preservation

In addition to conservation, a second important ingredient for statistical mechanics is the preservation, by the flow map, of the phase space volume element. In this section we demonstrate that each of the discretizations from Section 3.2 is volume preserving. Let us define the matrix $D(\boldsymbol{a}) = \mathrm{diag}(\boldsymbol{a})$ to be the diagonal matrix whose diagonal elements are the components of the vector $\boldsymbol{a}$ (i.e. $D(\boldsymbol{a})_{ij} = a_i\delta_{ij}$).

Recall that for an ODE

$$\boldsymbol{y}' = \boldsymbol{f}(\boldsymbol{y})$$

the divergence of the vector field $\boldsymbol{f}$ satisfies

$$\mathrm{div}\boldsymbol{f} = \mathrm{tr}(\boldsymbol{f}'),$$

where $\boldsymbol{f}'$ denotes the Jacobian matrix of $\boldsymbol{f}$. In particular, for a matrix A, $\mathrm{div}A\boldsymbol{f}(\boldsymbol{y}) = \mathrm{tr}(A\boldsymbol{f}')$. Furthermore, for

$$\boldsymbol{y}' = \boldsymbol{f}(\boldsymbol{y}) = \boldsymbol{g}(\boldsymbol{y}) * \boldsymbol{h}(\boldsymbol{y})$$

it holds that

$$\boldsymbol{f}' = D(\boldsymbol{g})\boldsymbol{h}' + D(\boldsymbol{h})\boldsymbol{g}'.$$

In the following calculations we make ready use of the commutative and transpose properties of the trace $\mathrm{tr}(AB) = \mathrm{tr}(BA) = \mathrm{tr}(B^{\mathrm{T}}A^{\mathrm{T}})$. We also need the following properties of our discretization matrices. The difference operators D_x and D_y are given by symmetric finite difference stencils, are skew-symmetric and commute $D_xD_y - D_yD_x = 0$. The discrete inverse Laplacian matrix Δ_M^{-1} is symmetric and represents a (typically global) central finite difference stencil. In this case, the matrices $D_x\Delta_M^{-1}$ and $D_y\Delta_M^{-1}$ have zeros on the diagonal.

Let us write the discretizations (11)–(13) as functions of $\boldsymbol{q}$ only

$$J_0(\boldsymbol{q}) = (D_x\boldsymbol{q}) * (D_y\Delta_M^{-1}\boldsymbol{q}) - (D_y\boldsymbol{q}) * (D_x\Delta_M^{-1}\boldsymbol{q}), \tag{23}$$

$$J_E(\boldsymbol{q}) = D_x(\boldsymbol{q} * D_y\Delta_M^{-1}\boldsymbol{q}) - D_y(\boldsymbol{q} * D_x\Delta_M^{-1}\boldsymbol{q}), \tag{24}$$

$$J_Z(\boldsymbol{q}) = D_y((D_x\boldsymbol{q}) * \Delta_M^{-1}\boldsymbol{q}) - D_x\big((D_y\boldsymbol{q}) * \Delta_M^{-1}\boldsymbol{q}\big). \tag{25}$$

Proposition 3.1. *The vector fields defined by (23)–(25) and their average $J_{EZ} = (J_0 + J_E + J_Z)/3$ are divergence-free.*

Proof. We calculate, for (23),

$$\mathrm{div}J_0(\boldsymbol{q}) = \mathrm{tr}(D(D_y\Delta_M^{-1}\boldsymbol{q})D_x) + \mathrm{tr}(D(D_x\boldsymbol{q})D_y\Delta_M^{-1}) - \mathrm{tr}(D(D_x\Delta_M^{-1}\boldsymbol{q})D_y) - \mathrm{tr}(D(D_y\boldsymbol{q})D_x\Delta_M^{-1}) = 0, \tag{26}$$

since each term is the trace of the product of a diagonal matrix and a matrix with zero diagonal.

For (24),

$$\begin{aligned}\mathrm{div}J_E(\boldsymbol{q}) &= \mathrm{tr}(D_x[D(\boldsymbol{q})D_y\Delta_M^{-1} + D(D_y\Delta_M^{-1}\boldsymbol{q})]) - \mathrm{tr}(D_y[D(\boldsymbol{q})D_x\Delta_M^{-1} + D(D_x\Delta_M^{-1}\boldsymbol{q})])\\ &= \mathrm{tr}(D(\boldsymbol{q})[D_y\Delta_M^{-1}D_x - D_x\Delta_M^{-1}D_y]) + \mathrm{tr}(D_xD(D_y\Delta_M^{-1}\boldsymbol{q}) - D_yD(D_x\Delta_M^{-1}\boldsymbol{q})) = 0.\end{aligned}$$

The term in brackets in the last expression is identically zero by symmetry considerations.

Similarly, for (25) we have

$$\begin{aligned}\mathrm{div}J_Z(\boldsymbol{q}) &= \mathrm{tr}(D_y[D(\Delta_M^{-1}\boldsymbol{q})D_x + D(D_x\boldsymbol{q})\Delta_M^{-1}]) - \mathrm{tr}(D_x[D(\Delta_M^{-1}\boldsymbol{q})D_y + D(D_x\boldsymbol{q})\Delta_M^{-1}])\\ &= \mathrm{tr}(D(\Delta_M^{-1}\boldsymbol{q})[D_xD_y - D_yD_x]) + \mathrm{tr}(D(D_x\boldsymbol{q})\Delta_M^{-1}D_y - D(D_y\boldsymbol{q})\Delta_M^{-1}D_y) = 0.\end{aligned}$$

Finally, discretization *EZ* is divergence-free because it is a linear combination of divergence-free vector fields. □

4. Energy–enstrophy statistical theory

The equilibrium statistical mechanical theory for 2D ideal fluids was developed by Kraichnan [9], Salmon et al. [22] and Carnevale and Frederiksen [3]. It is based on a finite truncation of the spectral decomposition of the equations of motion. Statistical predictions are obtained for the truncated system, and these are extended to the infinite dimensional limit.

In this paper we would like to adapt the analysis to the semi-discretizations outlined in the previous section. For the discretization *EZ*, which conserves both energy and enstrophy, the analysis is identical to the spectral

case developed by Carnevale and Frederiksen [3]. Consequently, most of the material in Sections 4.1–4.3 is simply summarized from Chapters 7 and 8 of Majda and Wang [12]. In Section 4.4 we modify the statistical predictions of the energy–enstrophy theory to the cases of only one quantity conserved.

As previously noted, semi-discretization of (1) using the bracket (14) yields a system of M^2 ordinary differential equations having the Liouville property and two first integrals that approximate the energy (21) and enstrophy (22).[1] Due to the Liouville property, one can speak of transport of probability density functions by this semi-discrete flow, and consider equilibrium solutions to Liouville's equation. Any normalized function of the two first integrals is an equilibrium distribution.

We note in advance that a solution of the semi-discrete equations (15) is constrained to the intersection of hypersurfaces defined by the relevant first integrals of the discretization. The probability distributions obtained from the maximum entropy theory have nonzero probability everywhere in phase space, and as such, are a very crude approximation to the statistics of a single trajectory. Nonetheless, we will see that the maximum entropy theory accurately predicts the differences in long-term averages observed for the discretizations (12)–(14). More on this will be said in Section 5.2.

4.1. Mean field predictions

The equilibrium distribution of least bias maximizes entropy under the constraints imposed by conservation of energy and enstrophy. Let $\boldsymbol{X}$ parameterize the M^2 dimensional phase space; that is, each $\boldsymbol{X} \in R^{M\times M}$ corresponds to a particular realization of the grid function (or discrete field) $\boldsymbol{q}$. Consider the class of probability distribution $\rho : R^{M\times M} \to R$ on phase space, satisfying

$$\rho(\boldsymbol{X}) \geqslant 0, \int_{R^{M\times M}} \rho(\boldsymbol{X})\mathrm{d}\boldsymbol{X} = 1. \tag{27}$$

The least biased distribution ρ^* maximizes the entropy functional

$$\mathcal{S}[\rho] = -\int_{R^{M\times M}} \rho(\boldsymbol{X}) \log \rho(\boldsymbol{X})\mathrm{d}\boldsymbol{X} \tag{28}$$

under constraints on the ensemble averages of energy:

$$\mathcal{K}_E[\rho] = \int_{R^{M\times M}} E_M(\boldsymbol{X})\rho(\boldsymbol{X})\mathrm{d}\boldsymbol{X} - E_M^* = 0 \tag{29}$$

and enstrophy:

$$\mathcal{K}_Z[\rho] = \int_{R^{M\times M}} Z_M(\boldsymbol{X})\rho(\boldsymbol{X})d\boldsymbol{X} - Z_M^* = 0, \tag{30}$$

where E_M^* and Z_M^* are prescribed values. Additionally, there is the constraint implied by (27). Using the method of Lagrange multipliers, the maximizer is the Gibbs-like distribution (i.e. $\rho^* = \mathcal{G}$)

$$\mathcal{G}(\boldsymbol{X}) = C^{-1} \exp[-\alpha(Z_M(\boldsymbol{X}) + \mu E_M(\boldsymbol{X}))], \tag{31}$$

where C, α and μ are chosen to ensure (27), (29) and (30).

The expected value of a function $F(\boldsymbol{X})$ is the ensemble average of F with the measure $\mathcal{G}$, denoted

$$\langle F \rangle = \int_{R^{M\times M}} F(\boldsymbol{X})\mathcal{G}(\boldsymbol{X})\mathrm{d}\boldsymbol{X}.$$

The mean state is obtained from the observation

$$\left\langle \frac{\partial Z_M}{\partial \boldsymbol{X}} + \mu \frac{\partial E_M}{\partial \boldsymbol{X}} \right\rangle = \int_{R^{M\times M}} \left(\frac{\partial Z_M}{\partial \boldsymbol{X}} + \mu \frac{\partial E_M}{\partial \boldsymbol{X}} \right) C^{-1} \mathrm{e}^{-\alpha(Z_M(\boldsymbol{X}) + \mu E_M(\boldsymbol{X}))}\,\mathrm{d}\boldsymbol{X} = -\alpha^{-1} \int_{R^{M\times M}} \frac{\partial}{\partial \boldsymbol{X}} \mathcal{G}(\boldsymbol{X})\mathrm{d}\boldsymbol{X} = 0,$$

[1] All discretizations also conserve the discrete total circulation $C_M = \sum_{ij} q_{ij}$. Since C_M is a linear first integral, any standard integrator will conserve it exactly in time. A nonzero value of C_M will give a constant displacement in (32). For a periodic domain one may assume that $C_M = 0$ so that its effects can be ignored. We do so in the numerical experiments.

assuming $\mathcal{G}$ decays sufficiently fast at infinity. Since $\nabla_{\boldsymbol{q}} E_M = -\boldsymbol{\psi}$ and $\nabla_{\boldsymbol{q}} Z_M = \boldsymbol{q}$, the mean field relation

$$\langle \boldsymbol{q} \rangle = \mu \langle \boldsymbol{\psi} \rangle \tag{32}$$

follows. In other words, the ensemble averages of potential vorticity and stream function are linearly related. Combining (32) with the second relation of (1) yields a Helmholtz problem for the mean stream function given μ:

$$(\mu - \Delta_M)\langle \boldsymbol{\psi} \rangle = \boldsymbol{h}. \tag{33}$$

4.2. PV fluctuation predictions

In this section we adapt the point statistics of Majda and Wang [12] to yield predictions in terms of potential vorticity. The mean state (32) is a nonlinearly stable equilibrium [3]. Solutions to (1) may be decomposed into mean and fluctuation parts

$$\boldsymbol{q} = \langle \boldsymbol{q} \rangle + \boldsymbol{q}', \quad \boldsymbol{\psi} = \langle \boldsymbol{\psi} \rangle + \boldsymbol{\psi}', \quad \langle \boldsymbol{q} \rangle = \mu \langle \boldsymbol{\psi} \rangle.$$

The fluctuation quantities satisfy

$$\boldsymbol{q}'_t = J(\langle \boldsymbol{q} \rangle, \boldsymbol{\psi}') + J(\boldsymbol{q}', \langle \boldsymbol{\psi} \rangle) + J(\boldsymbol{q}', \boldsymbol{\psi}'), \quad \Delta_M \boldsymbol{\psi}' = \boldsymbol{q}'. \tag{34}$$

This differential equation has the first integral

$$I_M(\boldsymbol{q}') = Z'_M + \mu E'_M, \quad Z'_M = \frac{1}{2}(\boldsymbol{q}')^{\mathrm{T}} \boldsymbol{q}' \Delta x \Delta y, \quad E'_M = -\frac{1}{2}(\boldsymbol{\psi}')^{\mathrm{T}} \boldsymbol{q}' \Delta x \Delta y. \tag{35}$$

One can also set up a statistical mechanics for the fluctuation equations and obtain predictions. To do so, let

$$\hat{p}_{k,\ell} = \left(1 + \frac{\mu}{k^2 + \ell^2}\right)^{1/2} \hat{q}'_{k,\ell}. \tag{36}$$

Then the Fourier transform of (35) gives

$$I_M = \frac{1}{2} \sum_{k,\ell} \left(1 + \frac{\mu}{k^2 + \ell^2}\right) |\hat{q}'_{k,\ell}|^2 \Delta x \Delta y = \frac{1}{2} \sum_{k,\ell} |\hat{p}_{k,\ell}|^2 \Delta x \Delta y = \frac{1}{2} \sum_{i,j} p_{i,j}^2 \Delta x \Delta y. \tag{37}$$

The maximum entropy condition for this first integral yields the Gibbs distribution $\mathcal{G}(\boldsymbol{p}) = C^{-1} \exp[-\beta I_M(\boldsymbol{p})]$, which is the product of identical Gaussian distributions with mean zero and standard deviation

$$\sigma_p = \sqrt{\frac{2\langle I_M \rangle}{M^2 \Delta x \Delta y}} = \sqrt{\frac{\langle I_M \rangle}{2\pi^2}}.$$

The energy is equipartitioned.

Let us also assume that the $p_{i,j}$ are independent. Let $P = \boldsymbol{a}^{\mathrm{T}} \boldsymbol{p}$ denote a linear combination of the $p_{i,j}$. Since these are identically distributed, P is Gaussian with variation

$$\sigma(P)^2 = \boldsymbol{a}^{\mathrm{T}} \boldsymbol{a} \sigma_p^2 = |\boldsymbol{a}|^2 \sigma_p^2.$$

From (36) we have

$$\boldsymbol{q}' = \mathcal{F}^{-1} \mathrm{diag}\left(\left(1 + \frac{\mu}{k^2 + \ell^2}\right)^{-1/2}\right) \mathcal{F} \boldsymbol{p} = A \boldsymbol{p},$$

where A is real and symmetric. It follows that the $q'_{i,j}$ at grid points i, j are identically normally distributed with mean zero and variance

$$\sigma_q^2 = |\boldsymbol{a}|^2 \sigma_p^2 = |\boldsymbol{a}|^2 \frac{\langle I_M \rangle}{2\pi^2}, \tag{38}$$

where for $\boldsymbol{a}$ we can take any row of A.

4.3. Approximation of μ and α

The ensemble averages of energy and enstrophy can be split into a mean part and a fluctuation part [3,12]:

$$\langle E_M\rangle = E_M(\langle \boldsymbol{q}\rangle) + E'_M, \quad \langle Z_M\rangle = Z_M(\langle \boldsymbol{q}\rangle) + Z'_M, \tag{39}$$

where, using (33),

$$E_M(\langle \boldsymbol{q}\rangle) = -\frac{1}{2}\langle \boldsymbol{\psi}\rangle^{\mathrm{T}}(\langle \boldsymbol{q}\rangle - \boldsymbol{h})\Delta x\Delta y = \frac{1}{2}\sum_{k,\ell=-M/2+1}^{M/2}\frac{(k^2+\ell^2)|\hat{h}_{k,\ell}|^2}{(\mu+k^2+\ell^2)^2}\Delta x\Delta y, \tag{40a}$$

$$E'_M = \frac{1}{2\alpha}\sum_{k,\ell=-M/2+1}^{M/2}\frac{1}{\mu+k^2+\ell^2} \tag{40b}$$

and

$$Z_M(\langle \boldsymbol{q}\rangle) = \frac{1}{2}\langle \boldsymbol{q}\rangle^{\mathrm{T}}\langle \boldsymbol{q}\rangle\Delta x\Delta y = \frac{1}{2}\sum_{k,\ell=-M/2+1}^{M/2}\frac{\mu^2|\hat{h}_{k,\ell}|^2}{(\mu+k^2+\ell^2)^2}\Delta x\Delta y, \tag{41a}$$

$$Z'_M = \frac{1}{2\alpha}\sum_{k,\ell=-M/2+1}^{M/2}\frac{k^2+\ell^2}{\mu+k^2+\ell^2}. \tag{41b}$$

Given guesses for μ and α, it is straightforward to compute $\langle E_M\rangle$ and $\langle Z_M\rangle$ by solving (40) and (41) and then substituting into (39). To estimate μ and α, we proceed iteratively to implicitly solve (29) and (30) under the assumptions $E^*_M \approx \mathcal{E}_0$ and $Z^*_M \approx \mathcal{Z}_0$.

4.4. Alternative statistical theories

In this section we derive alternative statistical models for the cases where either energy or enstrophy, but not both, is conserved numerically.

4.4.1. Energy-based statistical mechanics

For a semi-discretization that only preserves the energy E_M, the least biased distribution (31) becomes

$$\mathcal{G}_E(\boldsymbol{X}) = C^{-1}\exp\{-\lambda E_M(\boldsymbol{X})\}.$$

The mean field prediction (32) gives

$$\langle \boldsymbol{\psi}\rangle \equiv 0, \quad \langle \boldsymbol{q}\rangle = \boldsymbol{h}. \tag{42}$$

The fluctuation dynamics (34) becomes

$$\boldsymbol{q}'_t = J_E(\boldsymbol{h}+\boldsymbol{q}', \boldsymbol{\psi}'), \quad \boldsymbol{\psi}' = \Delta_M^{-1}\boldsymbol{q}',$$

which preserves the pseudo-energy

$$I_M = -\frac{1}{2}(\boldsymbol{\psi}')^{\mathrm{T}}\boldsymbol{q}'\Delta x\Delta y = E'_M \approx \mathcal{E}_0.$$

We define

$$\hat{p}_{k,\ell} = \frac{\hat{q}'_{k,\ell}}{(k^2+\ell^2)^{1/2}}.$$

The fluctuation Gibbs distribution is again Gaussian with $\sigma_p = (\langle I_M\rangle/2\pi^2)^{1/2}$. The fluctuation vorticity σ_q is given by (38) with $A = (-\Delta_M)^{1/2}$.

4.4.2. Enstrophy-based statistical mechanics

For a semi-discretization that only preserves the enstrophy Z_M, the least biased distribution (31) becomes

$$\mathcal{G}_E(\boldsymbol{X}) = C^{-1}\exp\{-\lambda Z_M(\boldsymbol{X})\}.$$

The mean field prediction (32) gives

$$\langle \boldsymbol{q}\rangle \equiv 0, \quad \langle \boldsymbol{\psi}\rangle = -\Delta_M^{-1}\boldsymbol{h}. \tag{43}$$

The fluctuation dynamics (34) becomes

$$\boldsymbol{q}' = J_Z(\boldsymbol{q}', \langle\boldsymbol{\psi}\rangle + \boldsymbol{\psi}'), \quad \boldsymbol{\psi}' = \Delta_M^{-1}\boldsymbol{q}'$$

and the pseudo-energy is just the enstrophy, i.e.

$$I_M = \frac{1}{2}(\boldsymbol{q}')^{\mathrm{T}}\boldsymbol{q}'\Delta x\Delta y = Z'_M \approx \mathcal{Z}_0.$$

The fluctuation Gibbs distribution is Gaussian with $\hat{p}_{k,\ell} = \hat{q}'_{k,\ell}$ and

$$\sigma_q = \sqrt{\frac{\langle I_M\rangle}{2\pi^2}}.$$

5. Time integration

To test the statistical predictions of the previous section with computations, the semi-discretizations of Section 3 must be supplemented with a time stepping scheme. One would prefer to have a scheme that conserves the invariants E_M and Z_M in time whenever these are first integrals of the spatial discretization. Additionally, one would like to have a scheme that preserves volume. There is much literature on the preservation of first integrals under discretization; see [7] for an overview. Much less is known about preserving volume.

5.1. Time discretizations

Since both invariants E_M and Z_M of the discretizations are quadratic functions of $\boldsymbol{q}$, they are automatically conserved if the equations are integrated with a Gauss–Legendre Runge–Kutta method [7]. The simplest such method is the implicit midpoint rule

$$\frac{\boldsymbol{q}^{n+1}-\boldsymbol{q}^n}{\Delta t} = J\left(\frac{\boldsymbol{q}^{n+1}+\boldsymbol{q}^n}{2}, \frac{\boldsymbol{\psi}^{n+1}+\boldsymbol{\psi}^n}{2}\right).$$

The discretization is also symmetric, and in the case of zero topography $h(\boldsymbol{x}) \equiv 0$, preserves the time reversal symmetry $t \mapsto -t$, $q \mapsto -q$ of (1). Although it is symplectic for Hamiltonian systems with constant structure operators, the midpoint rule is not volume preserving in general. Indeed, it does not preserve volume exactly for our discretizations. However, numerical experiments indicate that volume is approximately conserved on long intervals, even for a relatively large step size.

The implicit midpoint rule requires the solution of a nonlinear system of dimension M^2 at every time step. As a more efficient alternative, we can take any explicit Runge–Kutta method and project the solution onto the integral manifolds as desired. Let the Runge–Kutta method be represented by a map $\boldsymbol{q}^{n+1} = \Phi_{\Delta t}(\boldsymbol{q}^n)$ and compute a predicted step

$$\boldsymbol{q}^* = \Phi_{\Delta t}(\boldsymbol{q}^n).$$

Then project $\boldsymbol{q}^*$ onto the desired constraint manifolds by solving

$$\boldsymbol{q}^{n+1} = \boldsymbol{q}^* + \boldsymbol{g}'(\boldsymbol{q}^*)^{\mathrm{T}}\boldsymbol{\lambda},$$
$$\boldsymbol{g}(\boldsymbol{q}^{n+1}) = 0$$

for $\boldsymbol{\lambda}$, where $\boldsymbol{g}(\boldsymbol{q}) : R^{M\times M} \to R^r$, r the number of first integrals, and $\boldsymbol{\lambda} \in R^r$ is a vector of Lagrange multipliers. For example, we can take ($r = 3$)

$$\boldsymbol{g}(\boldsymbol{q}) = \begin{pmatrix} E_M(\boldsymbol{q}) - \mathcal{E}_0 \\ Z_M(\boldsymbol{q}) - \mathcal{Z}_0 \\ \left(\sum_{i,j} q_{i,j}\right) - 1 \end{pmatrix},$$

where the last constraint ensures that there is no drift in total vorticity. At each time step, projection requires solving a small nonlinear problem of dimension r. Projected Runge–Kutta methods will not preserve volume in general.

5.2. Time averages

Our interest is in the statistics applied to numerical data obtained from simulations over long times. To apply the theory from the previous sections, we additionally have to assume that the semi-discrete dynamics are ergodic. Denote the time average of a quantity $F(\boldsymbol{q}(t))$ by

$$\overline{F}_T = \frac{1}{T}\int_{t_0}^{t_0+T} F(\boldsymbol{q}(t))\mathrm{d}t.$$

Then the assumption of ergodicity implies that the long time average converges to the ensemble average

$$\overline{F} = \lim_{T\to\infty} \overline{F}_T = \langle F \rangle.$$

On the other hand, suppose one chooses discrete initial conditions to have a prescribed energy and enstrophy consistent with the continuum problem, i.e.

$$E_M(\boldsymbol{q}(0)) = \mathcal{E}_0, \quad Z_M(\boldsymbol{q}(0)) = \mathcal{Z}_0.$$

Then it is clear that since $E_M(\boldsymbol{q}(t)) = E_M(\boldsymbol{q}(0))$ and $Z_M(\boldsymbol{q}(t)) = Z_M(\boldsymbol{q}(0))$ are conserved, the dynamics only samples at most a codimension two subspace of $R^{M\times M}$, so one may ask to what extent the averages will converge. Indeed, one has inequality

$$\overline{E}_M = \langle E_M \rangle \neq \mathcal{E}_0, \quad \overline{Z}_M = \langle Z_M \rangle \neq \mathcal{Z}_0,$$

in general. By analogy with molecular dynamics, the Gibbs distribution (31) determines expectations in the canonical ensemble, whereas a constant energy–enstrophy simulation determines expectations in the microcanonical ensemble (assuming ergodicity). It is only in the 'thermodynamic limit' $M \to \infty$ that these averages coincide, giving equality in the above relations.

6. Numerical experiments

For the numerical experiments we use the test problem of [1]. The grid resolution is $M = 22$. The orography is a function of x only, specifically

$$h(x, y) = 0.2\cos x + 0.4\cos 2x.$$

(As a result the predicted mean fields $\bar{\boldsymbol{q}}$ and $\bar{\boldsymbol{\psi}}$ should be functions of x only.) The integrations were carried out using a step size of $\Delta t = 0.1$.

For initial conditions we take a uniformly random field[2] $\boldsymbol{q} = (q_{i,j}), i, j = 1, \ldots, M$ and project this onto the constraints

$$E_M(\boldsymbol{q}) = \mathcal{E}_0, \quad Z_M(\boldsymbol{q}) = \mathcal{Z}_0, \quad \sum_{i,j} q_{i,j} = 0.$$

The same initial condition is used for all simulations. The discrete energy and enstrophy were taken to be $\mathcal{E}_0 = 7$ and $\mathcal{Z}_0 = 20$.

[2] Experiments with smooth initial conditions typically show no noticable difference, however.

With these values prescribed, the statistical predictions of Section 4 can be computed for the three discretizations (12)–(14). The Lagrange multiplier μ is computed using the procedure described at the end of Section 4.3. Fluctuation statistics apply to the time series of PV at an arbitrarily chosen monitor point on the grid $q_{\text{mon}} = q_{3,12}$.

For the energy–enstrophy theory we obtain the mean state (32) and estimates

$$EZ : \mu = -0.730, \quad \langle q_{\text{mon}} \rangle = -0.341, \quad \sigma_q = 0.970. \tag{44}$$

For the energy theory of Section 4.4.1 we obtain the mean state (42) and estimates

$$E : \langle \psi \rangle \equiv 0, \quad \langle q_{\text{mon}} \rangle = 0.0740, \quad \sigma_q = 5.36. \tag{45}$$

For the enstrophy theory of Section 4.4.2 we obtain the mean state (43) and estimates

$$Z : \mu = 0, \quad \langle q_{\text{mon}} \rangle = 0, \quad \sigma_q = 1.01. \tag{46}$$

The discretization (11), which conserves neither energy nor enstrophy, was found to be exponentially unstable under time discretization by the implicit midpoint rule, and no experiments with that discretization will be reported here.

6.1. Results using implicit midpoint

We first present results obtained using the implicit midpoint discretization in time. The nonlinear relations were solved using fixed point iteration to a tolerance of 10^{-13}, which was the smallest tolerance that gave convergence at each step size for all discretizations. The solutions were averaged over the interval $10^3 \leqslant t \leqslant T$, for $T = 10^4, 10^5$ and 10^6. Averages were computed from time $t = 1000$ to allow the initially uniformly random initial condition to de-correlate, and this time is consistent with that used in [1] for a spectral discretization.

Given the average fields $\bar{\boldsymbol{q}}$ and $\bar{\boldsymbol{\psi}}$, the best linear fit to (32) yields an estimate of the Lagrange multiplier μ, i.e.

$$\bar{\mu} = \frac{\bar{\boldsymbol{\psi}}^{\mathrm{T}} \bar{\boldsymbol{q}}}{\bar{\boldsymbol{\psi}}^{\mathrm{T}} \bar{\boldsymbol{\psi}}}.$$

The relative change in energy and enstrophy for each discretization is plotted in Fig. 1 on the interval $[0, 10^4]$. The relative change is defined as

$$\Delta E_M^n = \frac{E_M^n - \mathcal{E}_0}{\mathcal{E}_0}, \quad \Delta Z_M^n = \frac{Z_M^n - \mathcal{Z}_0}{\mathcal{Z}_0}.$$

For the EZ discretization, both quantities are conserved up to the tolerance of the fixed point iteration, which leads to a small drift of magnitude 3×10^{-11} (relative) over this interval. For the E discretization, energy is conserved to the tolerance of the fixed point iteration, but enstrophy makes a rapid jump to a mean state roughly 30 times its initial value and subsequently undergoes bounded fluctuations with amplitude about $10 \times Z_0$. In contrast, for the Z discretization, enstrophy is similarly conserved, but energy drifts gradually with a negative trend, to about 25% of its initial value.

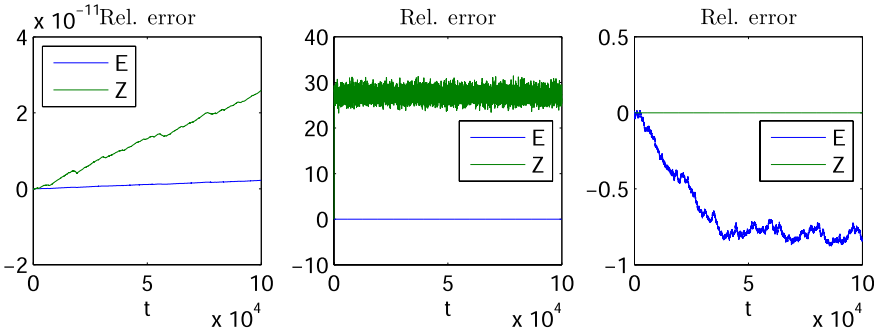

Fig. 1. Relative change in energy and enstrophy with EZ (left), E (middle) and Z (right) discretizations.

6.1.1. Long time mean fields

The time averaged stream function $\bar{\boldsymbol{\psi}}$ obtained by averaging over the interval $[10^3, 10^4]$ is shown in Fig. 2 for the three EZ, E and Z discretizations. Also shown is a scatter plot of the locus $(\bar{\psi}_{i,j}, \bar{q}_{i,j})$ and a linear best fit to this data for the respective discretizations.

For the EZ discretization, the mean stream function is similar to that predicted by the energy–enstrophy statistical theory (32), with $\bar{\mu} = -0.734$. For the E discretization, the mean stream function satisfies $\bar{\boldsymbol{\psi}} \approx 0$, consistent with (42), and the linear regression is inaccurate. For the Z discretization, we observe a similar mean state with $\bar{\mu} = -0.715$ on this averaging interval, which is inconsistent with prediction (46).

In Figs. 3 and 4 we examine more closely the mean fields for the EZ and Z discretizations, for longer averaging times of $T = 10^5$ and $T = 10^6$. For the energy–enstrophy discretization (14) in Fig. 3, the mean field

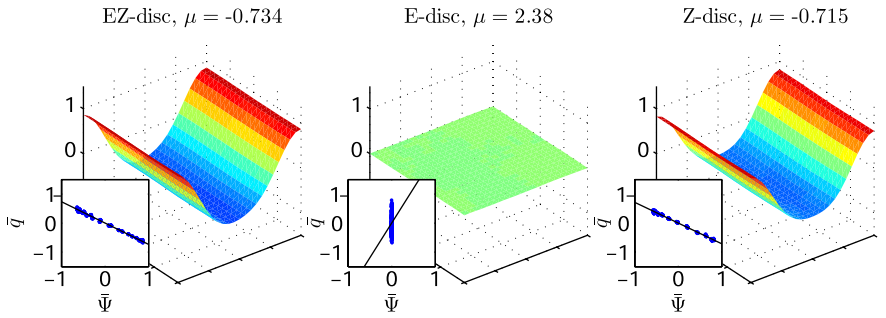

Fig. 2. Mean fields with averaging time 10^4, EZ (left), E (middle) and Z (right). The insets show the best linear fit to the relation $\bar{q}_{i,j} = \mu\bar{\psi}_{i,j}$ at all grid points.

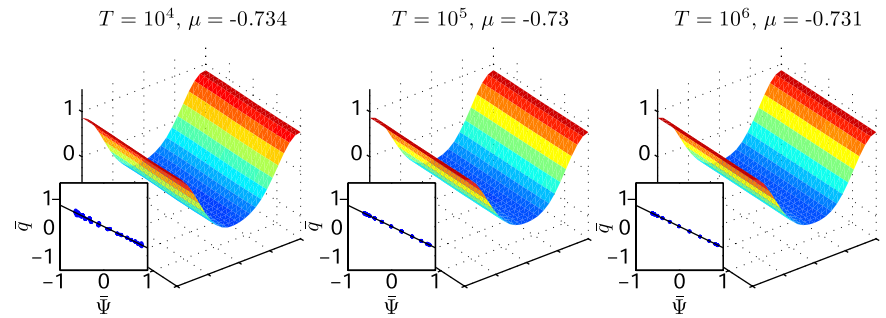

Fig. 3. Mean fields for EZ discretization with averaging times 10^4 (left), 10^5 (middle) and 10^6 (right). The insets show the best linear fit to the relation $\bar{q}_{i,j} = \mu\bar{\psi}_{i,j}$ at all grid points.

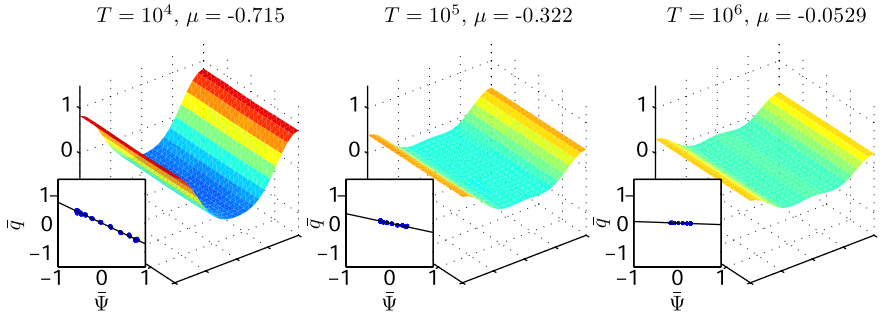

Fig. 4. Mean fields for discretization J_Z with averaging times 10^4 (left), 10^5 (middle) and 10^6 (right). The insets show the best linear fit to the relation $\bar{q}_{i,j} = \mu\bar{\psi}_{i,j}$ at all grid points.

appears to converge to an equilibrium state with $\bar{\mu} \approx -0.732$. The tendency in Fig. 4 is toward a mean field with zero vorticity, consistent with (43). However the relaxation time is much longer than for the other discretizations. For $T = 10^6$, the mean flow has $\bar{\mu} = -0.0529$. Note that the relation $\bar{\boldsymbol{q}} = \mu\bar{\boldsymbol{\psi}}$ approximates the data well for all averaging times, however. In Section 6.1.3 below, we show that the convergence of the Z discretization is in agreement with the EZ predictions on short time intervals, so that we can think of the system staying near statistical equilibrium with slowly drifting energy.

6.1.2. PV fluctuation statistics

In Fig. 5, the time series for potential vorticity q_{mon} at an arbitrarily chosen grid point (3, 12) is analyzed. As discussed in Section 4.2, the statistical theory for fluctuations predicts that the PV should be distributed normally about the mean field according to (44)–(46). For the longest simulation time of $T = 10^6$, the EZ discretization exhibits Gaussian fluctuations with mean $\bar{q}_{\text{mon}} = -0.395$ and standard deviation $\sigma = 0.927$; the E discretization with mean $\bar{q}_{\text{mon}} = -0.0093$ and standard deviation $\sigma = 5.35$; and the Z discretization with mean $\bar{q}_{\text{mon}} = -0.0575$ and standard deviation $\sigma = 1.05$. These observations are approximately in agreement with (44)–(46).

We mention that the value $\bar{\mu} = 0.732$, to which the EZ discretization seems to relax, corresponds to a mean energy value of $\langle E_N \rangle = 7.07$. For this value of mean energy, the prediction of Section 4.2 gives $\sigma = 0.928$, which is much closer to the value observed in Fig. 5. This indicates that for implicit midpoint, the mean energy is somewhat perturbed from the microcanonical energy $\mathcal{E}_0$.

6.1.3. Time-dependent energy–enstrophy model

In Fig. 6, the convergence of $\bar{\mu}$ is plotted as a function of averaging interval T for both the Z and EZ discretizations. The EZ dynamics relaxes very rapidly to give $\bar{\mu} \approx -0.73$, whereas the Z dynamics converges

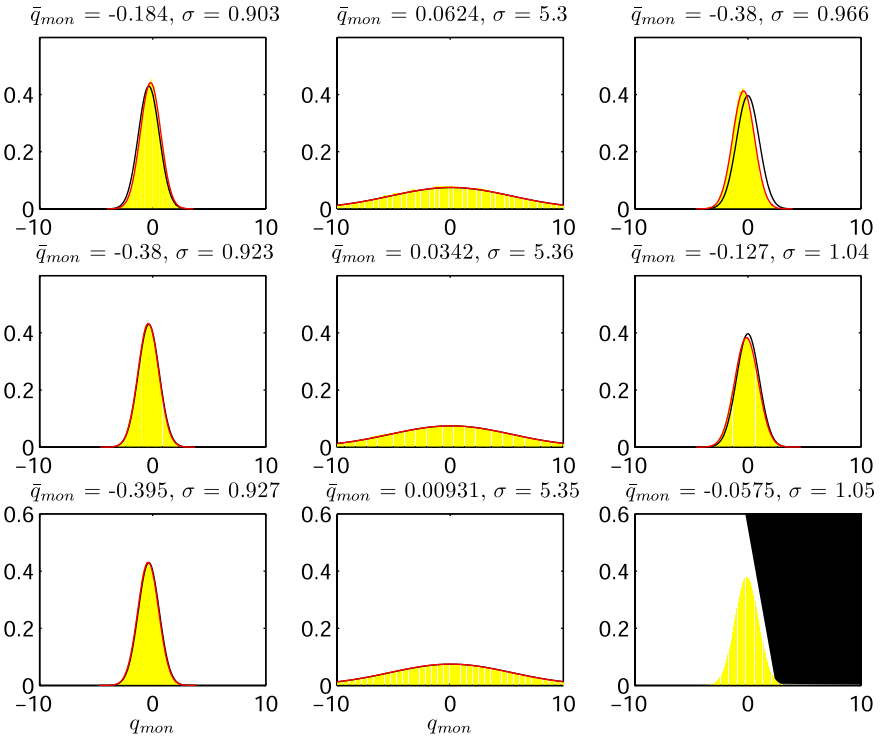

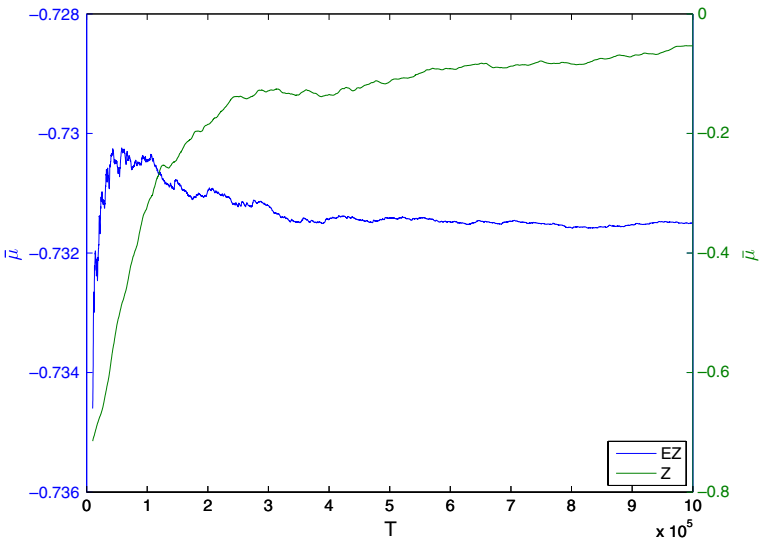

Fig. 6. Convergence of parameter μ_T as a function of the averaging interval T for the EZ and Z discretizations.

rather slowly towards $\bar{\mu} = 0$. Given the relatively fast relaxation of the energy–enstrophy conserving discretization to statistical equilibrium (32) and the slow drift of energy in Fig. 1 for the enstrophy conserving discretization (13), a natural model for the approach to equilibrium would be to consider a state $\bar{q}_T = \bar{\mu}_T \bar{\psi}_T$ with $\bar{\mu}_T$ corresponding to the instantaneous energy $E_M(T)$.

To test this idea, we define

$$\bar{\boldsymbol{\psi}}_T = \frac{1}{N_T}\sum_{n=1}^{N_T} \boldsymbol{\psi}^n, \quad \bar{\boldsymbol{q}}_T = \frac{1}{N_T}\sum_{n=1}^{N_T} \boldsymbol{q}^n,$$

where $T = N_T \cdot \Delta t$, and

$$\mu_T = \frac{(\bar{\boldsymbol{\psi}}_T)^{\mathrm{T}} \bar{\boldsymbol{q}}_T}{(\bar{\boldsymbol{\psi}}_T)^{\mathrm{T}} \bar{\boldsymbol{\psi}}_T}.$$

The energy of the associated equilibrium state is denoted $E_M(\bar{\mu}_T)$ and is determined from the relations in Section 4.3. This energy is plotted in Fig. 7 next to the actual discrete energy function, for increasing averaging intervals $T = 10, T = 100$ and $T = 1000$. The agreement supports this model. That is, the Z dynamics relaxes on a fast time scale to the statistical equilibrium predicted by energy–enstrophy theory *for the instantaneous energy*, while the energy drifts on a slow time scale towards the equilibrium state predicted by the enstrophy theory.

6.2. Results using projected Heun's method

Besides preserving quadratic first integrals exactly, the implicit midpoint rule is symmetric. It is unclear what effect, if any, this may have on statistics. Furthermore, the implicit midpoint rule is fully implicit and therefore not a very practical choice for integrating a nonstiff system such as (1). For these reasons we repeat the experiments of the previous section using the second order, explicit Runge–Kutta method due to Heun [8], coupled with projection onto the discrete energy and/or enstrophy manifolds. It should be recalled that Heun's method is linearly unstable with respect to a center equilibrium, and it is only due to projection that we can carry out long integrations with this method.

Fig. 8 compares the convergence of the parameter $\bar{\mu}_T$ as a function of T for the implicit midpoint and projected Heun integrators for the EZ and Z discretizations. In both cases, it appears that the projected method approaches equilibrium faster than implicit midpoint.

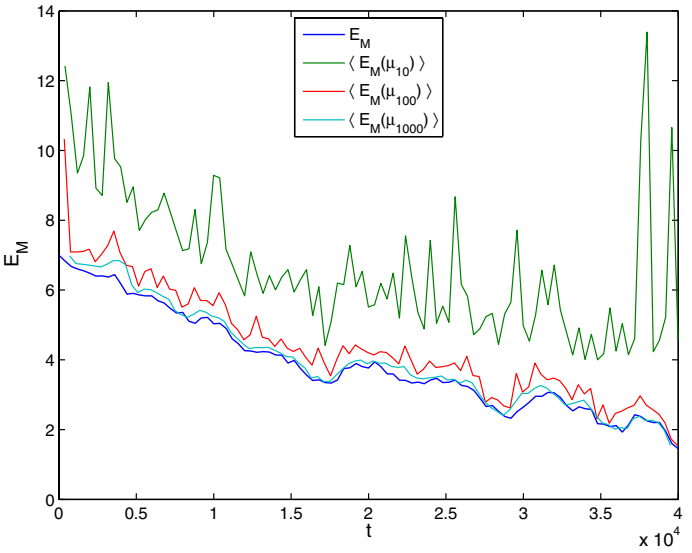

Fig. 7. Energy drift with Z discretization, compared to the energy associated with the best linear fit μ_T with averaging intervals $T = 10$, $T = 100$ and $T = 1000$.

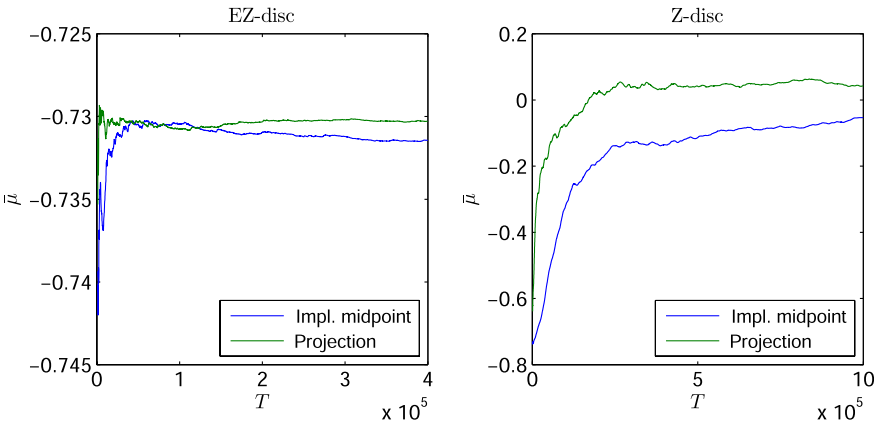

Fig. 8. Convergence of μ_T as a function of averaging interval T for EZ (left) and Z (right) discretizations, comparing the projected Heun's method and implicit midpoint.

Figs. 9–11 are analogous to Figs. 2–4 for implicit midpoint. Again we note that the projected method converges more rapidly and more accurately to the mean states (44)–(46).

The fluctuation statistics for the projection method are illustrated in Fig. 12. Here, too, we see that the projection method is very close to the statistically predicted value for mean and standard deviation of PV fluctuations in (44)–(46). However, it is important to note that since a measure of predictability is the *deviation from the statistical equilibrium*, a numerical method that approaches equilibrium excessively fast is undesirable from a prediction perspective.

6.3. Discrete volume preservation

Although the spatial discretizations were shown to be volume preserving, neither the implicit midpoint rule nor the projected Heun integrator preserves volume for the discrete map. To get an impression of the degree of volume contraction, we computed the determinant of the Jacobian of the discrete flow maps, e.g.

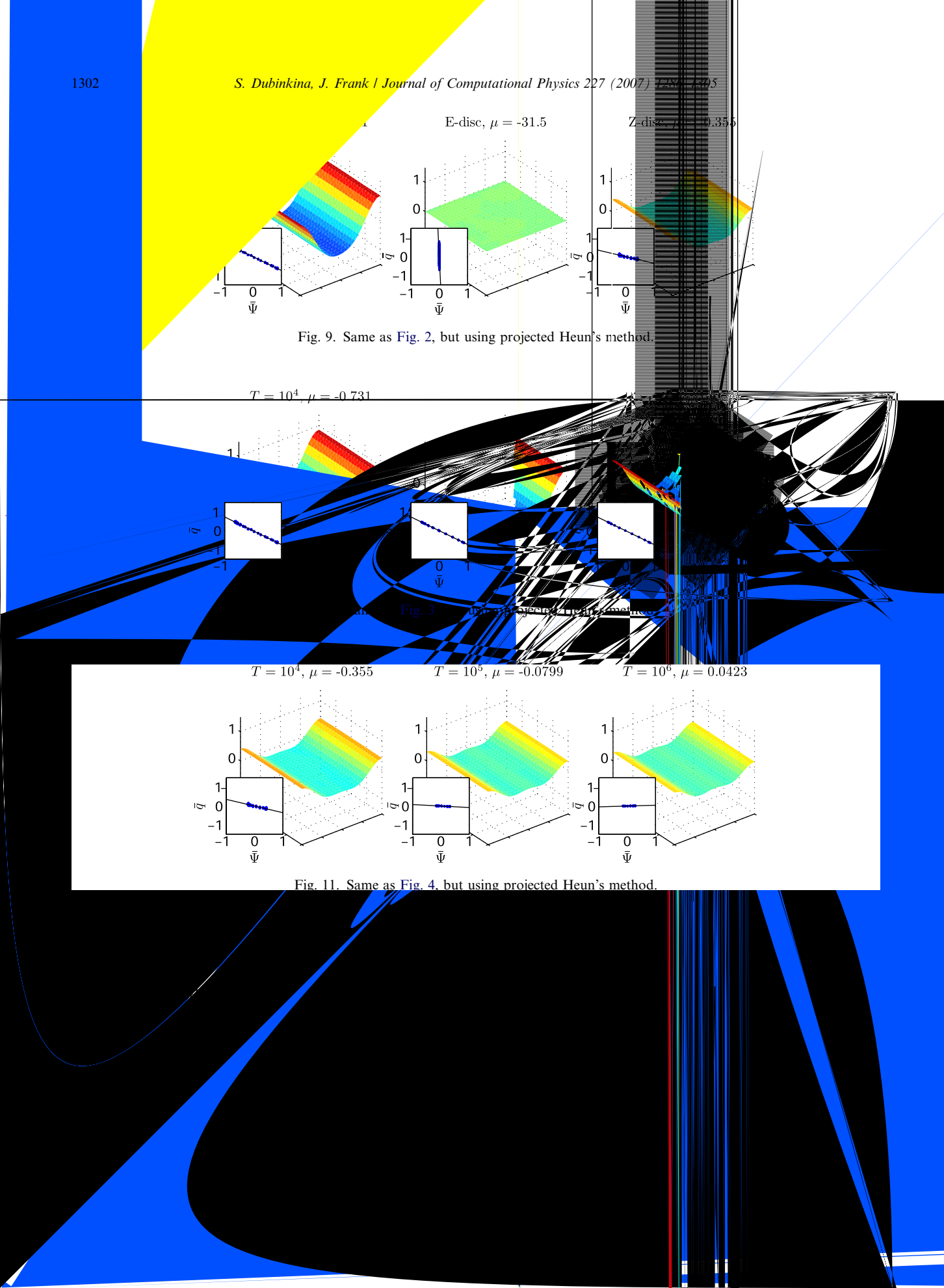

Fig. 9. Same as Fig. 2, but using projected Heun's method.

Fig. 3 [illegible] projected Heun's method.

Fig. 11. Same as Fig. 4, but using projected Heun's method.

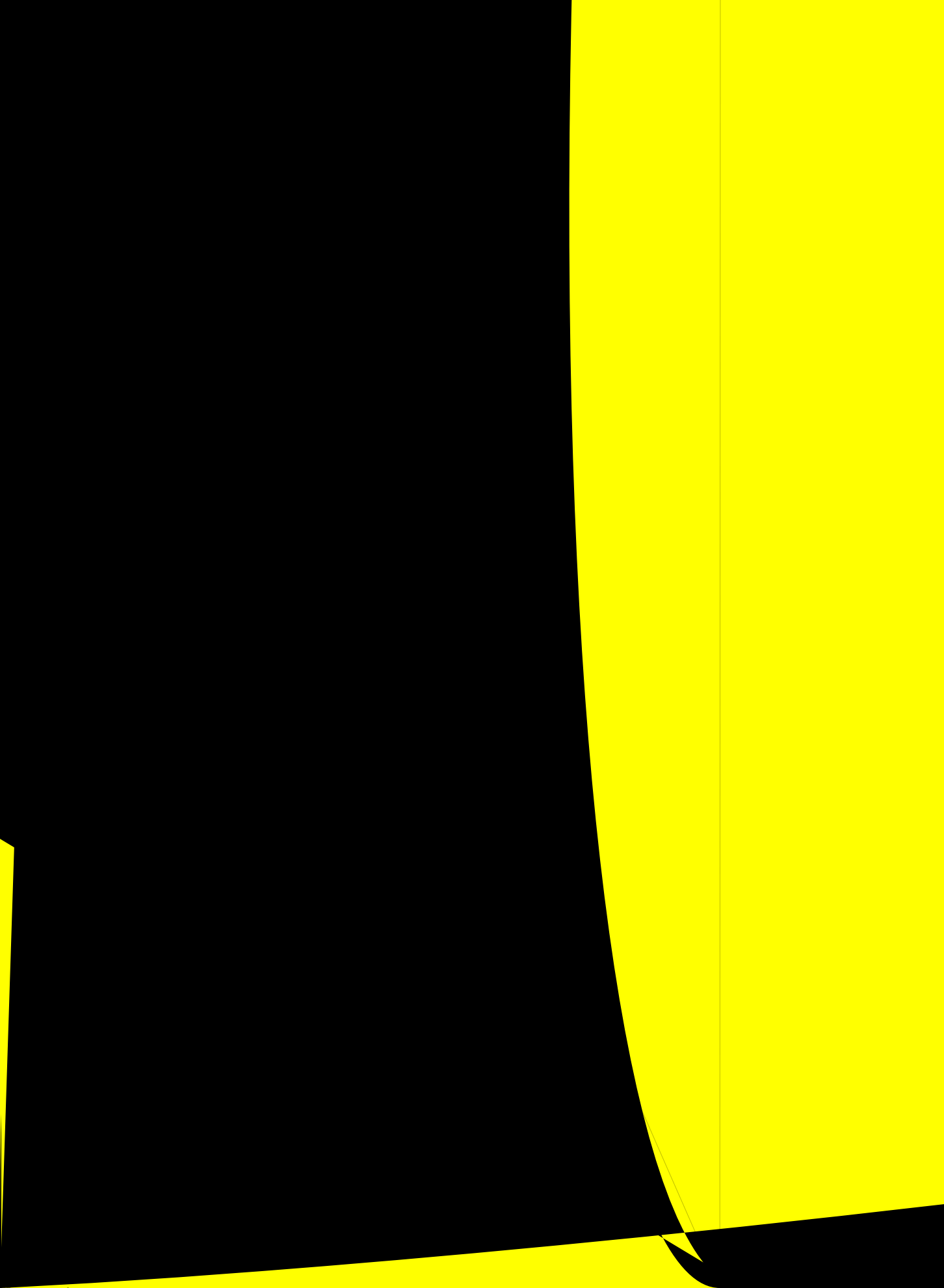

jected Runge–Kutta method. Long time averages with the implicit midpoint discretization relax to the predicted equilibrium at a slower rate than for the projected method, suggesting that implicit midpoint has higher potential for prediction. The implicit midpoint rule was also found to approximately conserve volume for long time intervals. This is in stark contrast to the projection method, for which phase space volume is rapidly contracted.

The three statistical theories predict dramatically different behavior, and this is confirmed by the numerical experiments. In other words, *the three discretizations exhibit dramatically different behavior* in simulations over long intervals. The statistical equilibrium states define a backdrop on which the discrete dynamics occurs, and that backdrop depends on the conservation properties of the spatial discretization. Assuming the energy–enstrophy theory to be correct, it is thus essential for any code to preserve both quantities (under semi-discretization) if statistical consistency is desired.

On the other hand, it has been shown by Abramov and Majda [1] that the energy–enstrophy theory is incomplete. In [1], the Poisson discretization of [26] is integrated using the Poisson splitting of McLachlan [14]. The semi-discretization preserves, in addition to the Hamiltonian, M Casimirs corresponding to the first M moments of potential vorticity (PV), and these are preserved by the splitting (the energy is only preserved approximately, in the sense of backward error analysis [7]). Abramov and Majda give convincing evidence that nonzero values of the third moment of PV, when conserved by the discretization, can significantly skew the predictions of the standard theory of [9,22,3,12].

Nonetheless, the results of this paper make a strong argument for the use of conservative discretizations in weather and climate simulations.

Planned further work on the subjects of this paper will address shallow water equations on the sphere, energy and enstrophy conserving discretizations [23,20,21], and the Hamiltonian Particle-Mesh method [4–6], a symplectic discretization of inviscid fluids. In [5] it is shown that the HPM method satisfies a circulation theorem, but it is uncertain to what extent this can be interpreted as enstrophy conservation. We expect the current approach will clarify this issue.

Acknowledgements

We wish to acknowledge helpful discussions with Stephen Bond and Jacques Vanneste at the ''Applying Geometric Integrators Workshop'', held at the ICMS in Edinburgh in April 2007. Sebastian Reich gave us invaluable feedback. We also thank Alex Vonk for his work on the projection methods, and Jan Verwer for constructive remarks.

References

[1] R.V. Abramov, A.J. Majda, Statistically relevant conserved quantities for truncated quasigeostrophic flow, Proc. Natl. Acad. Sci. USA 100 (7) (2003) 3841–3846 (electronic).
[2] A. Arakawa, Computational design for long-term numerical integration of the equations of fluid motion: two-dimensional incompressible flow. Part I., J. Comput. Phys. 1 (1966) 119–143.
[3] G.F. Carnevale, J.S. Frederiksen, Nonlinear stability and statistical mechanics of flow over topography, J. Fluid Mech. 175 (1987) 157–181.
[4] J. Frank, G. Gottwald, S. Reich, A Hamiltonian particle-mesh method for the rotating shallow-water equations, in: Meshfree Methods for Partial Differential Equations (Bonn, 2001), Lect. Notes Comput. Sci. Eng., vol. 26, Springer, Berlin, 2003, pp. 131–142.
[5] J. Frank, S. Reich, Conservation properties of smoothed particle hydrodynamics applied to the shallow water equation, BIT 43 (1) (2003) 41–55.
[6] J. Frank, S. Reich, The Hamiltonian particle-mesh method for the spherical shallow water equations, Atmos. Sci. Lett. 5 (2004) 89–95.
[7] E. Hairer, C. Lubich, G. Wanner, Geometric numerical integration, Springer Series in Computational Mathematics, second ed., vol. 31, Springer-Verlag, Berlin, 2006, structure-preserving algorithms for ordinary differential equations.
[8] E. Hairer, S.P. Nørsett, G. Wanner, Solving Ordinary Differential Equations. I, Springer Series in Computational Mathematics, second ed., vol. 8, Springer-Verlag, Berlin, 1993, nonstiff problems.
[9] R.H. Kraichnan, Statistical dynamics of two-dimensional flow, J. Fluid Mech. 67 (1975) 155–175.
[10] B. Leimkuhler, S. Reich, Simulating Hamiltonian dynamics, Cambridge Monographs on Applied and Computational Mathematics, vol. 14, Cambridge University Press, Cambridge, 2004.
[11] E.N. Lorenz, Energy and numerical weather prediction, Tellus 12 (1960) 364–373.

[12] A.J. Majda, X. Wang, Non-linear Dynamics and Statistical Theories for Basic Geophysical Flows, Cambridge University Press, Cambridge, 2006.
[13] R. McLachlan, Symplectic integration of Hamiltonian wave equations, Numer. Math. 66 (4) (1994) 465–492.
[14] R.I. McLachlan, Explicit Lie-Poisson integration and the Euler equations, Phys. Rev. Lett. 71 (19) (1993) 3043–3046.
[15] P.J. Morrison, Hamiltonian description of the ideal fluid, Rev. Modern Phys. 70 (2) (1998) 467–521.
[16] Y. Nambu, Generalized Hamiltonian dynamics, Phys. Rev. D 7 (3) (1973) 2405–2412.
[17] P. Névir, R. Blender, A Nambu representation of incompressible hydrodynamics using helicity and enstrophy, J. Phys. A 26 (22) (1993) L1189–L1193.
[18] J. Pedlosky, Geophysical Fluid Dynamics, second ed., Springer, 2005.
[19] R. Salmon, Lectures on Geophysical Fluid Dynamics, Oxford University Press, New York, 1998.
[20] R. Salmon, Poisson-bracket approach to the construction of energy- and potential-enstrophy-conserving algorithms for the shallow-water equations, J. Atmos. Sci. 61 (16) (2004) 2016–2036.
[21] R. Salmon, A general method for conserving quantities related to potential vorticity in numerical models, Nonlinearity 18 (5) (2005) R1–R16.
[22] R. Salmon, G. Holloway, M.C. Hendershott, The equilibrium statistical mechanics of simple quasi-geostrophic models, J. Fluid Mech. 75 (1976) 691–703.
[23] R. Salmon, L.D. Talley, Generalizations of Arakawa's Jacobian, J. Comput. Phys. 83 (2) (1989) 247–259.
[24] J.M. Sanz-Serna, M.P. Calvo, Numerical Hamiltonian problems, Applied Mathematics and Mathematical Computation, vol. 7, Chapman & Hall, London, 1994.
[25] A.M. Stuart, A.R. Humphries, Dynamical systems and numerical analysis, Cambridge Monographs on Applied and Computational Mathematics, vol. 2, Cambridge University Press, Cambridge, 1996.
[26] V. Zeitlin, Finite-mode analogs of 2D ideal hydrodynamics: coadjoint orbits and local canonical structure, Physica. D 49 (3) (1991) 353–362.